Journal of Environmental Management 200 (2017) 366–379

Contents lists available at ScienceDirect

Journal of Environmental Management

journal homepage: www.elsevier.com/locate/jenvman

Research article

Coupling distributed stormwater collection and managed aquifer recharge: Field application and implications

S. Beganskas*, A.T. Fisher

University of California, Santa Cruz, United States

ARTICLE INFO

Article history:
Received 16 February 2017
Received in revised form
17 May 2017
Accepted 19 May 2017

Keywords:
Managed aquifer recharge
Distributed stormwater collection
Groundwater management
Precipitation intensity
Infiltration capacity
Sediment accumulation

ABSTRACT

Groundwater is increasingly important for satisfying California's growing fresh water demand. Strategies like managed aquifer recharge (MAR) can improve groundwater supplies, mitigating the negative consequences of persistent groundwater overdraft. Distributed stormwater collection (DSC)–MAR projects collect and infiltrate excess hillslope runoff before it reaches a stream, focusing on 40–400 ha drainage areas (100–1000 ac). We present results from six years of DSC–MAR operation—including high resolution analyses of precipitation, runoff generation, infiltration, and sediment transport—and discuss their implications for regional resource management. This project generated significant water supply benefit over six years, including an extended regional drought, collecting and infiltrating 5.3×10^5 m^3 (426 ac-ft). Runoff generation was highly sensitive to sub-daily storm frequency, duration, and intensity, and a single intense storm often accounted for a large fraction of annual runoff. Observed infiltration rates varied widely in space and time. The basin-average infiltration rate during storms was 1–3 m/d, with point-specific rates up to 8 m/d. Despite efforts to limit sediment load, 8.2×10^5 kg of fine-grained sediment accumulated in the infiltration basin over three years, likely reducing soil infiltration capacity. Periodic removal of accumulated material, better source control, and/or improved sediment detention could mitigate this effect in the future. Regional soil analyses can maximize DSC–MAR benefits by identifying high–infiltration capacity features and characterizing upland sediment sources. A regional network of DSC–MAR projects could increase groundwater supplies while contributing to improved groundwater quality, flood mitigation, and stakeholder engagement.

1. Introduction

Worldwide, groundwater is an increasingly vital and limited resource (Gleeson et al., 2010; Wada et al., 2010, 2012; Richey et al., 2015). In California, water demand consistently exceeds available surface supplies, increasing reliance on groundwater (California Department of Water Resources, 1998a, 2013). Data from 2001 to 2010 show growing statewide water shortages, including large groundwater deficits even during wet years (Table 1); the 2012–15 California drought further stressed water resources (Griffin and Anchukaitis, 2014; Asner et al., 2016). Groundwater overdraft, which occurs when aquifer outputs (including groundwater extraction) persistently exceed inputs, has many negative consequences (Konikow and Kendy, 2005; Zektser et al., 2005; Werner et al., 2013; Döll et al., 2014). Overdraft has caused saltwater intrusion, subsidence, and permanent storage loss in California's aquifers (Galloway et al., 1998; Nenna et al., 2013; Faunt et al., 2016). California enacted its first statewide groundwater management legislation in 2014, the Sustainable Groundwater Management Act, which creates a framework for local agencies to bring groundwater basins into balance. However, the best way to augment resources remains unclear in many basins (Nelson, 2012). Timely research on methods to improve water supply and quality will facilitate effective water management solutions.

Managed aquifer recharge (MAR) can improve groundwater supply and quality (Lee et al., 1992; Ma and Spalding, 1997; Scanlon et al., 2016) by introducing excess surface water into underlying

* Corresponding author.
E-mail address: sbegansk@ucsc.edu (S. Beganskas).

http://dx.doi.org/10.1016/j.jenvman.2017.05.058
0301-4797/

Table 1
Data from the Department of Water Resources show large deficits in California's water budget, especially for groundwater.

CA Water Plan Update		Normal [a]		Dry [a]		Wet [a]	
		(km^3)	(Maf)	(km^3)	(Maf)	(km^3)	(Maf)
1998[b]	1995: Δ*Supply*	−2.0	−1.6	−6.3	−5.1	n.d.	n.d.
	2020: Δ*Supply* (projected)	−0.2	−0.2	−3.3	−2.7	n.d.	n.d.
2013[c]	2001–2010: Δ*Supply*	−9.9	−8.0	−19.4	−15.7	−0.6	−0.5
	2001–2010: Δ*GW*	−11.1	−9.0	−14.7	−11.9	−6.3	−5.1

[a] Calculated and projected annual imbalances between fresh water supply and demand under normal, dry, and wet conditions. Maf = millions of acre feet. Δ*Supply* is all fresh water resources, Δ*GW* is just groundwater.
[b] Values as listed in Table 10-4 (California Department of Water Resources, 1998a), with normal and dry conditions defined using data collected through WY1995. This assessment did not include environmental flows or evaluation of wet conditions.
[c] Based on values listed in Table 3-2 (California Department of Water Resources, 2013) for WY2001–WY2010, including environmental flows. Data were aggregated, defining normal years as having 80–120% of historical mean precipitation, dry years as having <80%, and wet years as having >120%. This table included no future projections, and was based on a ten-year period preceding the recent drought.

aquifers with subsequent municipal, agricultural, and/or environmental benefit (Bouwer, 1999, 2002; Dillon, 2005; Dillon et al., 2010). MAR methods to move surface water into aquifers include infiltration basins, farm field flooding, stream bank filtration, and injection wells (Doussan et al., 1998; Pavelic et al., 2006; O'Geen et al., 2015).

Changing precipitation patterns provide new opportunities to develop MAR projects using stormwater. Numerous studies have reported increasing precipitation intensity over the last century, including analyses of California, Europe, East Asia, and the Middle East (Tomozeiu et al., 2000; Lenderink and van Meijgaard, 2008; Leahy and Kiely, 2011; Tu and Chou, 2013; Furl et al., 2014; Kaźmierczak and Kotowski, 2014; Zhang and Cong, 2014; Zolina, 2014). A recent study of extreme precipitation in the San Francisco Bay Area, just north of the present study's field site, found that mean annual precipitation changed little in the last 120 years, whereas large storms became less frequent and more intense (Russo et al., 2013). More intense precipitation tends to generate more runoff, resulting in less infiltration and recharge. These patterns are influenced by decadal-scale climate cycles (Shang et al., 2011; Jong et al., 2016) and may be associated with anthropogenic climate change (Zhang et al., 2007; Liu et al., 2009; Min et al., 2011; Mahlstein et al., 2012). Urbanization also contributes to increased runoff generation and decreased recharge, creating stormwater management challenges (National Research Council, 2008; Cantone and Schmidt, 2011; Wright et al., 2012; Chaffin et al., 2016; Jia et al., 2016). Collecting and infiltrating excess runoff can mitigate flooding and help bring groundwater basins into balance.

This study focuses on distributed stormwater collection (DSC), which involves collecting excess hillslope runoff during storms before it reaches a stream. Gravity routes the runoff to an infiltration site (e.g., basin, drywell), where it percolates to an underlying aquifer. DSC–MAR bridges a gap in scale between two common MAR practices: low impact development (LID) and regional spreading grounds. LID collects runoff close to the source in small structures, generally in urban areas. While costs can be modest, individual LID projects infiltrate relatively little: ~10^3 m^3/yr (~1 ac-ft/yr) (Stephens et al., 2012; Grebel et al., 2013; Newcomer et al., 2014; Bhaskar et al., 2016; Chen et al., 2016). Regional spreading grounds infiltrate excess surface and/or recycled water from large regions, collecting and routing water with dams and other large infrastructure. Regional projects may infiltrate >10^7 m^3/yr (>10^5 ac-ft/yr), but are complex to design and build, require a steady water supply, and are expensive to operate (Clark et al., 2004; Quast et al., 2006). We focus on DSC–MAR projects with drainage areas of 40–400 ha (100–1000 ac) and infiltration basins of 0.4–4 ha (1–10 ac). Projects in this size range are intended to be developed rapidly, engineered with modest landscape modification, and maintained at low cost, while generating enough infiltration benefit (≥10^5 m^3/yr, ≥100 ac-ft/yr per site) to justify the effort.

We present results from six years of DSC–MAR operation in a groundwater basin suffering from overdraft. Field analyses provide valuable ground-truth for models evaluating locations for future MAR projects (Saraf and Choudhury, 1998; Jha et al., 2007; Yeh et al., 2009; Chenini et al., 2010; Rahman et al., 2012, 2013; Russo et al., 2014) and elucidate important site conditions that may not be represented in regional studies. We analyze the dynamics of, and relations between, precipitation, runoff generation, infiltration, and sediment transport at this site and discuss broader water resource management implications.

2. Setting and methods

2.1. Pajaro Valley Groundwater Basin

The Pajaro Valley Groundwater Basin (PVGB) is located in southern Santa Cruz County and northern Monterey County along California's central coast (Fig. 1A), a region that meets 85% of water demand with groundwater (California Department of Water Resources, 2013). The PVGB underlies the topographic basins of the lower Pajaro River watershed and the Elkhorn Slough watershed (U.S. Geological Survey, 2014), bounded to the north and east by the Santa Cruz Mountains and the San Andreas Fault, to the south by the Seaside and Salinas Groundwater Basins, and to the west by Monterey Bay and the Pacific Ocean.

Groundwater is particularly important in the PVGB, which lacks both seasonal snow pack and surface water imports (Hanson et al., 2014b). Most groundwater extracted (~6.4×10^7 m^3/yr, ~5.2×10^4 ac-ft/yr) is used for agricultural irrigation. Given the mild climate and loose, well-drained soils, agriculture is especially productive in the PVGB, generating >$800 million/yr in revenue (Hanson et al., 2014a). The Pajaro River is a losing stream in the PVGB (Ruehl et al., 2006; Hatch et al., 2010). However, groundwater provides baseflow for tributaries, including Corralitos Creek, which are critical habitat for Steelhead Trout (*Oncorhynchus mykiss*), a federally-listed anadromous fish species (Harding ESE, 2001; NOAA Fisheries, 2016). Amidst a growing population and expanding agricultural development, the PVGB has experienced overdraft for decades, depleting groundwater supply and leading to saltwater intrusion (Pajaro Valley Water Management Agency, 2014; Russo et al., 2014).

Annual precipitation over the last 75 years averaged 55 ± 20 cm/yr, with considerable spatial and interannual variability (California

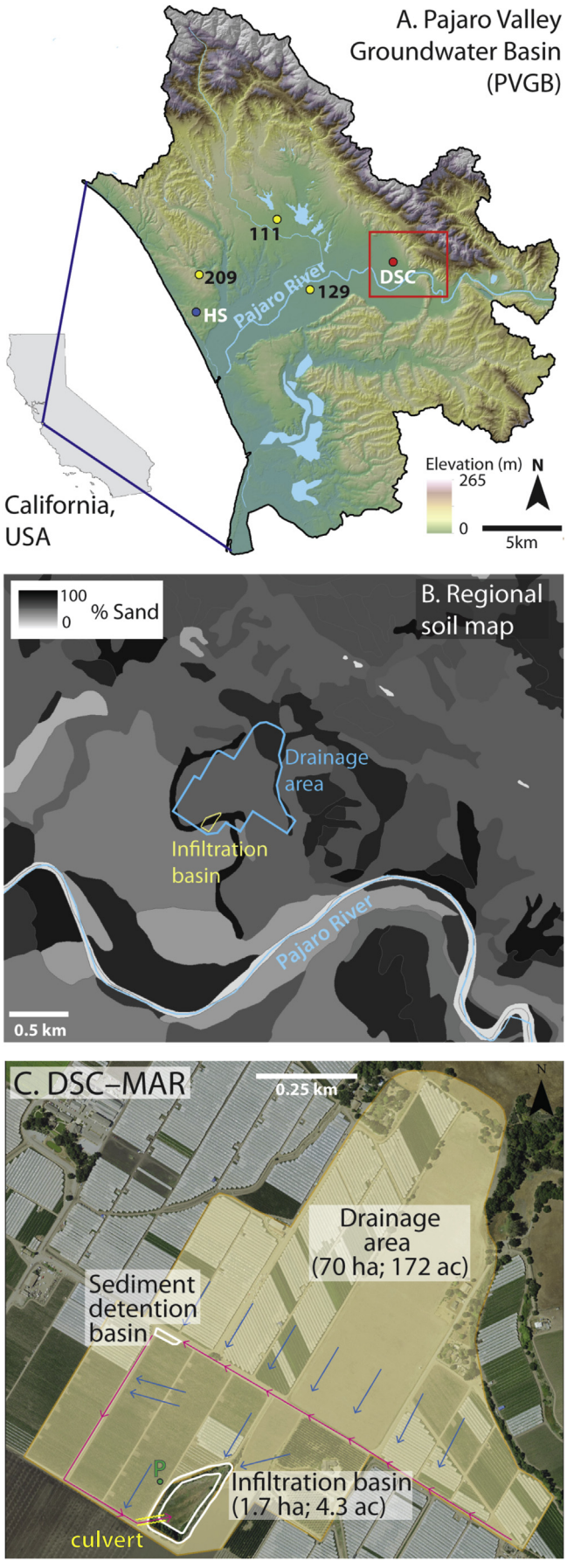

Department of Water Resources, 1998b). There is a strong north-to-south precipitation gradient across the PVGB, with ≥130 cm/yr falling to the north in the Santa Cruz Mountains and ≤50 cm/yr to the south. Precipitation is highly seasonal, with most rainfall occurring between November and April. As in much of the western U.S., the annual hydrologic cycle is assessed within water years (WY) that begin October 1 (e.g., WY14 = 1 October 2013 through 30 September 2014).

Annual overdraft in the PVGB is estimated to be 1.5×10^7 m^3/yr (1.2×10^4 ac-ft/yr) (Hanson et al., 2014a). The Pajaro Valley Water Management Agency is implementing a basin management plan to enhance supply (through wastewater recycling and MAR) and reduce demand (through conservation). The agency currently operates one MAR project, diverting water from Harkins Slough (Fig. 1A). The field site for this study is the first DSC–MAR project in the PVGB and others are in development.

2.2. Field site and instrumentation

The project is on an active ranch, where runoff from a drainage area of 70 ha (172 ac) is diverted into a 1.7-ha (4.3-ac) infiltration basin (Fig. 1C). Runoff would otherwise flow southwest to the Pajaro River and into Monterey Bay. Runoff from the upper drainage area flows into a sediment detention basin before being routed through a culvert to the infiltration basin. The infiltration basin was created by modifying a natural topographic depression, originally intended to limit runoff to adjacent properties. The southern third of the infiltration basin is underlain by Conejo clay loam and the northern two-thirds are underlain by Baywood loamy sand, which appears to be a paleochannel (Fig. 1B) (Soil Survey Staff, U.S. Department of Agriculture, 2014). Additional soil units in the drainage area include Conejo loam, Elkhorn sandy loam, and Pfeiffer gravelly sandy loam. The surrounding ranch grows a variety of crops, including strawberries, cane berries, and salad vegetables. The orientation and treatment of these fields vary between crop rotation and planting cycles, and fields are often tilled during the dry season.

We surveyed and instrumented this field site to elucidate hydrologic conditions and DSC–MAR performance during WY12–WY17. We measured and/or calculated precipitation, runoff collected, basin-average and point-specific infiltration rates, and sediment accumulation (Table S1 lists instrument metadata). In WY14, WY15, and WY17, some instruments were installed to telemeter data in real-time, allowing for remote project management, enhanced communication with project partners, and broader stakeholder engagement.

2.3. Precipitation and runoff

We measured precipitation with a tipping-bucket rain gauge (0.25 mm/tip) and converted tip dates/times into hourly rainfall

Fig. 1. Site maps show context and components for DSC–MAR project design. **A.** Topographic map overlying the PVGB, California, showing study location (*DSC*), local CIMIS stations (*111, 129,* and *209*), and the Harkins Slough MAR site (*HS*). *Red square* shows location of panel B. **B.** DSC–MAR infiltration basin (*yellow*) and drainage area (*blue*) overlain on a regional soil map (Soil Survey Staff, U.S. Department of Agriculture, 2014) colored by sand fraction (darker colors indicate sandier soil). The infiltration basin includes part of a sandy paleochannel. **C.** Aerial photograph of DSC–MAR project site. Runoff flows into a sediment detention basin, along farm roads, and through a culvert (*yellow*) into the infiltration basin (*pink arrows*, channelized flow; *blue arrows*, overland flow; *green dot, P*, rain gauge). (For interpretation of the references to colour in this figure legend, the reader is referred to the web version of this article.)

rates. We compared these records to hourly precipitation data from nearby California Irrigation Management Information System (CIMIS) weather stations (California Department of Water Resources, 1998b) at Pajaro (#129, 1996–2014), Green Valley Road (#111, 1993–2014), and Watsonville (#209, 2008–2014) (Fig. 1A). Five annual CIMIS records were eliminated due to significant data gaps during the rainy season, resulting in 43 station-years of data for comparison with field data.

We defined a rainfall "event" as ≥0.5 cm rain, below which field data suggests little runoff is generated. As winter precipitation in this region is characterized by multi-day storms separated by dry periods of days to weeks, we chose 24 h as the minimum inter-event time (Dunkerley, 2008). For each water year of field and CIMIS data, we calculated total annual precipitation, number of events, average event duration, average event precipitation intensity, maximum hourly precipitation intensity, and number of days with >0.5 cm rain.

We calculated the volume of runoff routed into the infiltration basin by relating water depth in the inflow culvert to flow rate using the Manning equation (Akgiray, 2005) (see SI). Calculations during WY14 suggested that the corrugated culvert with a 46-cm inner diameter was a flow bottleneck that could cause flooding. The grower installed a replacement culvert prior to WY15 with a larger diameter (91 cm) and smooth inner profile, providing greater discharge capacity. Calculations of runoff collected for infiltration are likely conservative, because runoff flowed into the basin around the sides at ungauged locations.

2.4. Infiltration rates

The daily (midnight-to-midnight) volume of infiltration, I_V, was calculated by mass balance:

$$I_V = Q_{\text{inflow}} + P - ET - \Delta S \quad (1)$$

where Q_{inflow} = volume of runoff flowing into the basin [L^3]
P = volume of precipitation [L^3]
ET = volume of evapotranspiration [L^3]
ΔS = net change in volume stored in the basin [L^3]

Q_{inflow} was calculated by integrating the time-series of calculated flow rates through the culvert. P was calculated by multiplying the infiltration basin area by precipitation depth recorded on-site. ET was calculated as the minimum of daily precipitation and potential evapotranspiration reported from local CIMIS stations (using the Penman–Monteith method), multiplied by the basin wetted area.

Storage in the infiltration basin was calculated using a digital elevation model (DEM) generated from survey data collected with a total station theodolite. The DEM was used to derive polynomial equations relating water stage to storage volume and wetted area. Absolute pressure gauges measured water stage at 15-min intervals, with local correction for barometric pressure. ΔS was calculated by comparing values at the start and end of each day. We calculated the daily basin-average infiltration rate by dividing I_V by the mean daily wetted basin area. We calculated point-specific vertical infiltration rates at multiple locations in the infiltration basin during WY13–15 using a heat as a tracer (Constantz and Thomas, 1996; Anderson, 2005; Constantz, 2008), based on the amplitude reduction of daily temperature fluctuations with depth (Hatch et al., 2006) (see SI).

2.5. Sediment transport and accumulation

In WY13–15, we used a hand auger to collect sediment samples up to 2 m below ground surface (bgs) from the upland drainage area, sediment detention basin, and infiltration basin. To assess how much sediment accumulated in the infiltration basin, we deployed collection trays (HDPE, 30-cm square, pebbled texture) at the start of WY13–15. We measured accumulated sediment depth on each tray at the end of the rainy season, created a contour map, and calculated the total volume of accumulated sediment. We converted volume to mass assuming a dry bulk density of 1700 kg/m^3 based on local soil data (Racz et al., 2011). For each water year, we combined sediment mass and runoff volume to calculate the average runoff sediment load and divided accumulated sediment mass by drainage area to calculate sediment yield.

We processed sediment samples to determine their grain size distributions (see SI) and used two-sample Kolmogorov–Smirnov (K–S) tests to compare grain size between sample pairs (Massey, 1951). We used the Kozeny–Carman equation (Chapuis, 2012) to calculate saturated vertical hydraulic conductivity (K [L/T]) based on the grain size distribution of individual samples:

$$\log K = 0.5 + \log \frac{e^3}{G^2 S^2 (1+e)} \quad (2)$$

where e = void ratio [−] = $\frac{n}{1-n}$
n = porosity [−] = 0.255 (1 + 0.83 U)
U = coefficient of grain size uniformity [−] = $\frac{d_{60}}{d_{10}}$
d_{60} = diameter for which 60% of grains are finer [L]
d_{10} = diameter for which 10% of grains are finer [L]
G = specific weight [−] = $\frac{\rho_{\text{sediment}}}{\rho_{\text{water}}}$
S = specific surface [L^2/M] (Chapuis and Aubertin, 2003)

We compared sediment properties to soil types in the Natural Resource Conservation Service SSURGO database (Soil Survey Staff, U.S. Department of Agriculture, 2014). For each sample location in the infiltration basin, we calculated effective hydraulic conductivity (K_{eff}) at the end of WY13–15 (see SI). Calculating K_{eff} allowed us to quantitatively relate changes in grain size to soil infiltration capacity. We also modeled how K_{eff} would change as fine-grained sediment accumulated on the ground surface.

3. Results

3.1. Precipitation and runoff

Annual precipitation at the field site was 26–90 cm/yr, consistent with the 75-year mean of 55 ± 20 cm/yr (California Department of Water Resources, 1998b). Precipitation was below average during WY12–15, when California was experiencing a severe drought (Mann and Gleick, 2015). The annual runoff coefficient (total runoff divided by total rainfall) during the study period varied from 0.01 (WY12) to 0.41 (WY15) and was not strongly correlated to total precipitation (Table 2). In WY12, there were a few widely separated precipitation events (Fig. 2A), the maximum culvert inlet water level was 0.11 m, and total runoff collected was 2200 m^3 (1.7 ac-ft). In WY13, most precipitation and all runoff occurred during December 2012 (Fig. 2B). Water levels at the culvert inlet reached 0.74 m, submerging the culvert for 2 h; total runoff collected was 3.8 × 10^4 m^3 (31 ac-ft). WY14 received the least total precipitation in this study, yet storms in February/March 2014 delivered very intense rainfall (Fig. 2C). Water levels at the culvert inlet peaked at 0.78 m, submerging the culvert for 5 h; total runoff collected was 4.2 × 10^4 m^3 (34 ac-ft). In WY15, intense storms in December 2014 delivered 20.5 cm of precipitation over ten days, with more than half of that (10.9 cm) falling in one day (Fig. 2D). Total runoff collected was 1.3 × 10^5 m^3 (107 ac-ft), more

Table 2
Aggregated data for each water year in this study.

	Total precipitation	Total runoff collected		Annual runoff coefficient	Water in infiltration basin	Thickness of sediment deposited	Mass of sediment deposited	Annual sediment load	Annual sediment yield	
	(cm)	(m^3)	(ac-ft)	–	(days)	(cm)	(kg)	(g/L)	(Mg/km^2)	(tons/acre)
WY2012	33.0	2200	1.7	0.01	n.d.	n.d.	n.d.	n.d.	n.d.	n.d.
WY2013	39.1	38,300	31.1	0.14	40	0–8	423,700	11.0	609	2.7
WY2014	25.6	41,900	34.0	0.24	43	0–1	83,400	2.0	120	0.5
WY2015	46.3	132,300	107.2	0.41	59	0–7	310,500	2.3	735	3.3
WY2016	69.5	135,200	109.6	0.28	105	n.d.	n.d.	n.d.	n.d.	n.d.
WY2017	89.7	175,400	142.2	0.28	72	n.d.	n.d.	n.d.	n.d.	n.d.

n.d. = no samples or data collected.

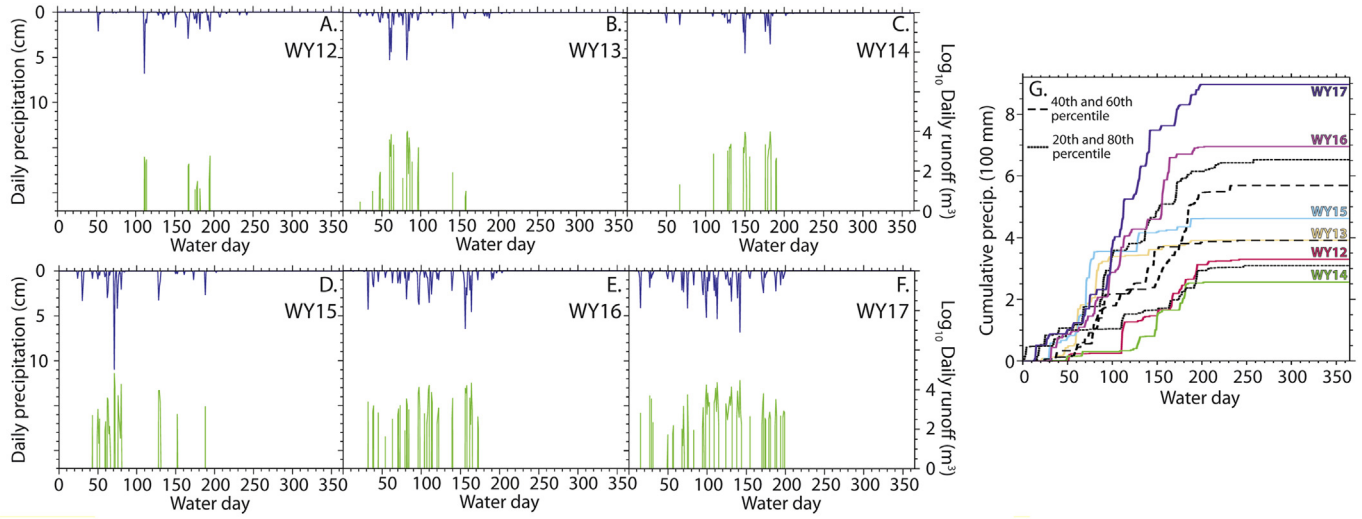

Fig. 2. Field data show that rainfall was below average during the first four years of the study. **A**–**F.** Daily precipitation (*left axis, top data*) and runoff (*right axis, bottom data*) plotted versus water day (1 October = water day 1). **G.** Cumulative daily precipitation for WY12–17 (*colored*), and 20th, 40th, 60th, and 80th percentile historical cumulative daily precipitation (*dotted and dashed black lines*) from three CIMIS stations (1993–2014).

than the previous three years combined. Precipitation was distributed more evenly throughout the wet season during WY16 and WY17, and in both years exceeded the 80th percentile of CIMIS records (Fig. 2E–G); total runoff collected was 1.5×10^5 m^3 (109 ac-ft) and 1.8×10^5 m^3 (143 ac-ft), respectively.

During WY15–17, runoff collection exceeded the project goal of 1.2×10^5 m^3/yr (100 ac-ft/yr). The larger culvert, installed before WY15, was never fully submerged, but water levels remained >0.46 m, the diameter of the old culvert, for 7 h during WY15. The ability of the larger-diameter culvert to accommodate rapid runoff accumulation during large storms, relative to the smaller culvert in previous years, highlights the benefits of carefully designing DSC–MAR projects to minimize flow bottlenecks.

Annual precipitation and runoff broadly correlated, though annual precipitation alone was an inaccurate predictor of DSC performance (Fig. 3). Although 50% more precipitation fell in WY13 than WY14, these years generated a similar amount of runoff. Similarly, WY15 and WY16 generated about the same volume of runoff, although 50% more precipitation fell in WY16. Conversely, although WY12 had 29% more precipitation than WY14, ~7.5 times as much runoff was generated in WY14. WY15 had just 18% more precipitation than WY13, but generated ~3.5 times more runoff.

A comparison of precipitation event characteristics elucidates these observations. WY14 had the least precipitation, but the long event duration and high event intensity generated more runoff relative to WY12; the latter had more rain but shorter and less intense events (Fig. 4A,B,D). More intense precipitation generates more runoff if the precipitation rate exceeds the soil infiltration capacity, causing infiltration-excess, or Hortonian, runoff (Horton, 1933; Wierda and Veen, 1992; Li et al., 2014). Variations in event duration and intensity help explain why comparable runoff volumes were collected in WY13 and WY14, although there were more events and more precipitation in WY13 (Fig. 4A,C); average event duration and intensity were much lower in WY13 (Fig. 4B,D).

Precipitation events were relatively long and intense in WY15 (Fig. 4B,D). Longer-duration precipitation generates more runoff if rainfall continues after soil pores fill with water, creating saturation-excess, or Dunnian, runoff (Dunne and Black, 1970; Li et al., 2014). This explains why more than three times as much runoff was generated in WY15 compared to WY13, even though WY13 had only 7.1 cm less precipitation than WY15, and a similar number of rainy days (Fig. 4A,F). The relatively large number of events in WY13 (Fig. 4C) means that there were few consecutive days with enough precipitation to generate runoff. Indeed, precipitation events in WY13 were the shortest recorded during the study (1.1 days in WY13 vs. 1.9 days in WY15) and among the shortest from CIMIS records (Fig. 4B).

Detailed storm characteristics (depth, duration, intensity) and

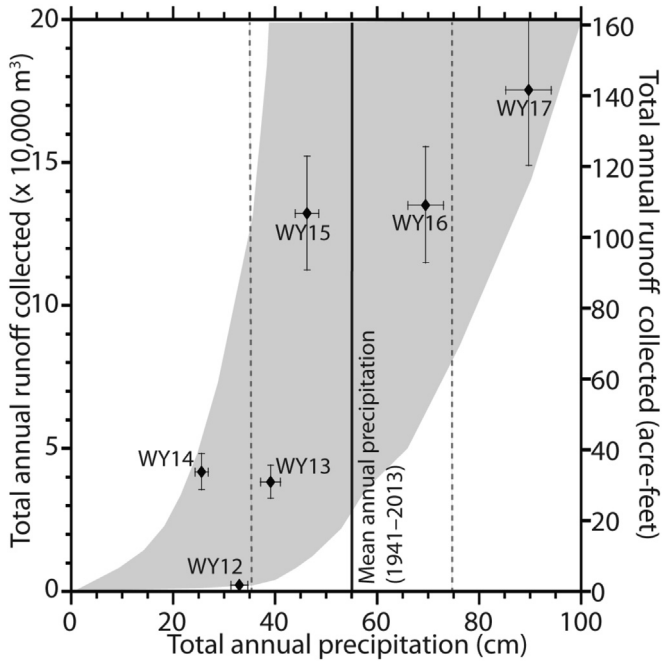

Fig. 3. Total annual runoff collected did not consistently correlate with total annual precipitation (*solid line*, mean annual precipitation; *dotted lines*, one standard deviation). The *gray band* projects a range of runoff this project could collect under different precipitation conditions.

soil properties influenced how much precipitation became runoff. Generally, more runoff was generated when one storm occurred soon after another storm, likely due to elevated antecedent soil moisture. While it is time-consuming and expensive to monitor soil moisture throughout a heterogeneous drainage basin, rainfall–runoff measurements provide a valuable, integrated record. In addition, differences between on-site precipitation records and nearby CIMIS records illustrate spatial variability in storm characteristics, and meaningful differences in storm characteristics that were apparent in hourly data were often obscured in aggregated daily (or longer) records. Local, high-resolution data collection can help develop accurate, site-specific rainfall–runoff relations needed to quantify DSC–MAR project viability and performance.

3.2. Water mass balance and infiltration dynamics

Mass-balance calculations indicated highly variable basin-average infiltration rates (Fig. 5). The average rate was 0.3 m/d, but as the basin filled during storms, rates increased to 1–3 m/d. On the day with most intense rainfall (10.9 cm/d) in WY15, basin stage peaked at >2 m, much higher than any other point during the study, and the infiltration rate was 7.8 m/d. Basin stage peaked at 1.5 m in WY17 and infiltration rates reached 5.7 m/d. In general, faster infiltration occurred on days with higher basin stage, likely because higher water pressure drove more rapid infiltration and a higher stage wetted the sandier, northern part of the basin. A conservative infiltration capacity estimate for this basin during storms is 1.5 m/d. Based on these observations, this system appears to be runoff-limited rather than infiltration capacity–limited. Across a wide range of natural events, the project worked as intended, and could likely handle even greater rates of runoff inflow before reaching system capacity.

According to mass balance calculations, rainy-day ET was seasonally less than 0.5% of infiltration. Similarly, evaporative losses comprised <2% of infiltration at the nearby Harkins Slough MAR site (Racz et al., 2011). These results make sense considering the high soil infiltration capacity and that infiltration of runoff occurs during winter rainfall, when it is cool and humid.

Point-specific infiltration rates, determined using heat as a tracer, varied spatially and temporally (Fig. 6). The time-series method was originally developed for measuring continuous infiltration over weeks to months (Hatch et al., 2006); edge effects equivalent to the order of the filter applied (2–3 days in the present study) made infiltration events shorter than 4–5 days difficult to resolve using this approach. The method worked well for long storms in WY15, and local infiltration patterns were generally consistent with basin-average rates. However, point-specific rates were often lower than basin-average rates, suggesting that thermal probes did not sample the fastest infiltration pathways (e.g., sand lenses, animal burrows, and root tubules).

The spatial distribution of infiltration rates varied throughout WY15 (Fig. 6). During the largest storm, infiltration was initially fastest along the southwest corner, where the basin is deepest. As the storm continued, basin stage rose, higher-elevation areas were inundated, and the region of fastest infiltration migrated northward towards sandier soils. Areas of rapid infiltration also shifted over time at the Harkins Slough MAR site, but over a ten-week period (Racz et al., 2011). Infiltration rates are influenced by many factors, including substrate texture and hydrologic properties, antecedent moisture, escape of trapped air, clogging, and water depth driving infiltration (Bouwer, 2002; Racz et al., 2011). Spatially and temporally variable infiltration rates have important water quality implications, as discussed later.

3.3. Sediment transport and accumulation

Sediment accumulation varied annually and spatially within the infiltration basin (Table 2, Fig. S1). Up to 8 cm of sediment accumulated in WY13 and WY15, with the greatest accumulation in the southern (deeper) half of the infiltration basin, close to the inlet. In WY13, 4.2×10^5 kg of sediment accumulated, with a mean runoff sediment load of 11 g/L; 3.1×10^5 kg accumulated in WY15, with a runoff sediment load of 2.3 g/L. In WY14, far less accumulated, 8.3×10^4 kg, but the runoff sediment load was 2 g/L, similar to WY15. Although runoff sediment loads were modest, the annual sediment yield of the drainage area, 120–735 Mg/km^2, is in the middle range of values from other agriculturally developed regions (Koluvek et al., 1993; de Vente and Poesen, 2005; Ficklin et al., 2010; García-Ruiz et al., 2013).

Grain size analyses showed that accumulating sediment had a different texture from both upland soil available for transport and subsurface soil in the infiltration basin. Upland soil samples had a typical mode of ~350 μm (Fig. 7A), with a small fraction of finer-grained material, 1–50 μm. Samples from 50 to 150 cm-bgs in the infiltration basin had similar grain size distributions to upland soil (Fig. 7C) and K–S test results are consistent with these two groups being drawn from a single population of samples. In contrast, sediment deposited in the basin during WY13–15 (collected on sediment trays) was much finer, with modes of 1–50 μm (Fig. 7B); K–S test results confirm this significant difference. These results suggest that finer sediments were preferentially transported and deposited in the infiltration basin, whereas coarser material was lost in transit or retained in the sediment detention basin. Grain size results showed an increase in fine grains (and decrease in coarse grains) in the infiltration basin subsurface over WY13–15 (Fig. 7C).

Fine-grained sediment accumulation in the infiltration basin had a long-term impact. In WY13, the median saturated hydraulic

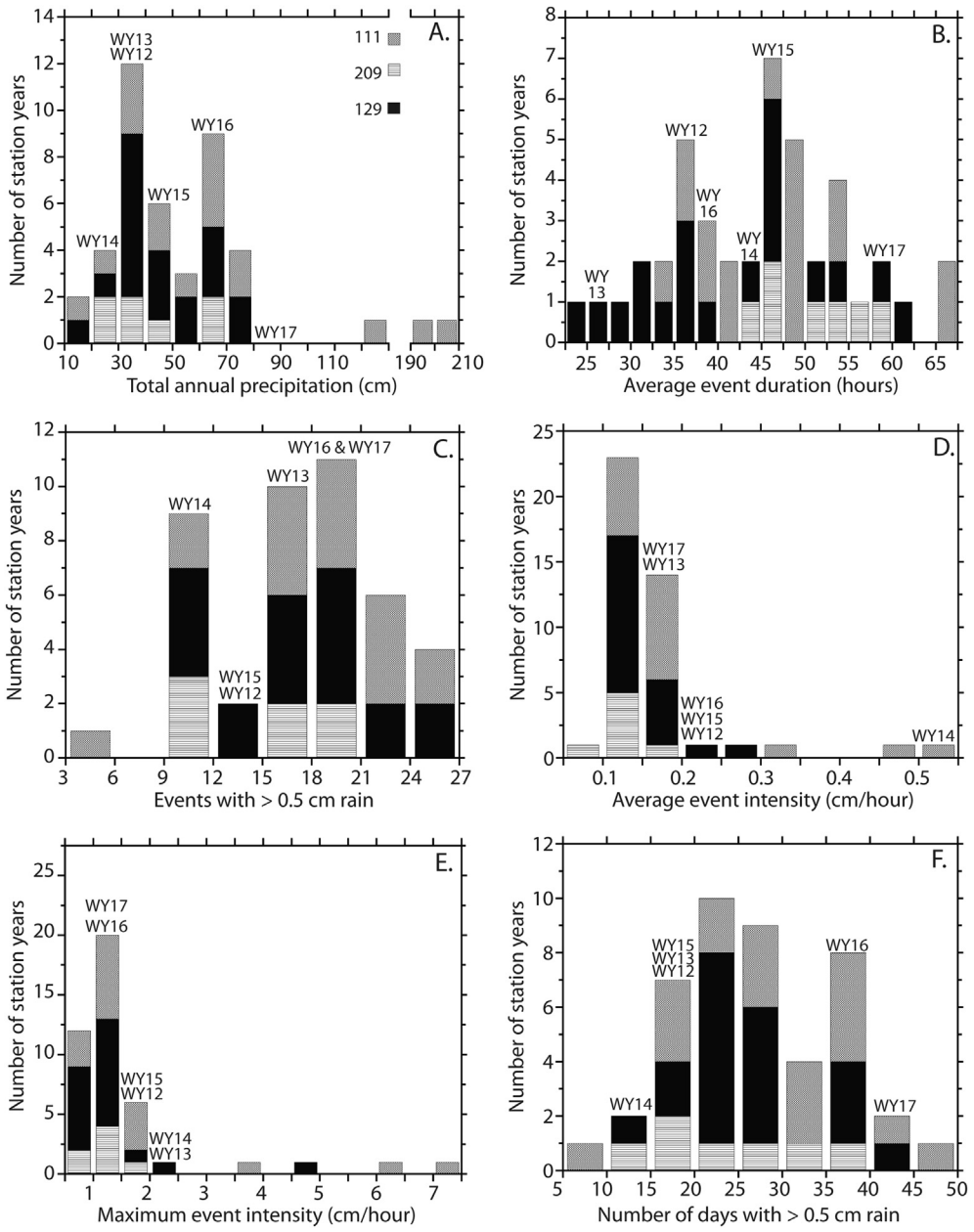

Fig. 4. Analyses of hourly precipitation data reveal important differences in rainfall characteristics during this study. **A–F.** Histograms of precipitation metrics for 43 years of CIMIS data (1993–2014; locations of 111, 129, and 209 shown on Fig. 1A). Labels indicate where the six years of this study's data (WY12–17) fall within these distributions.

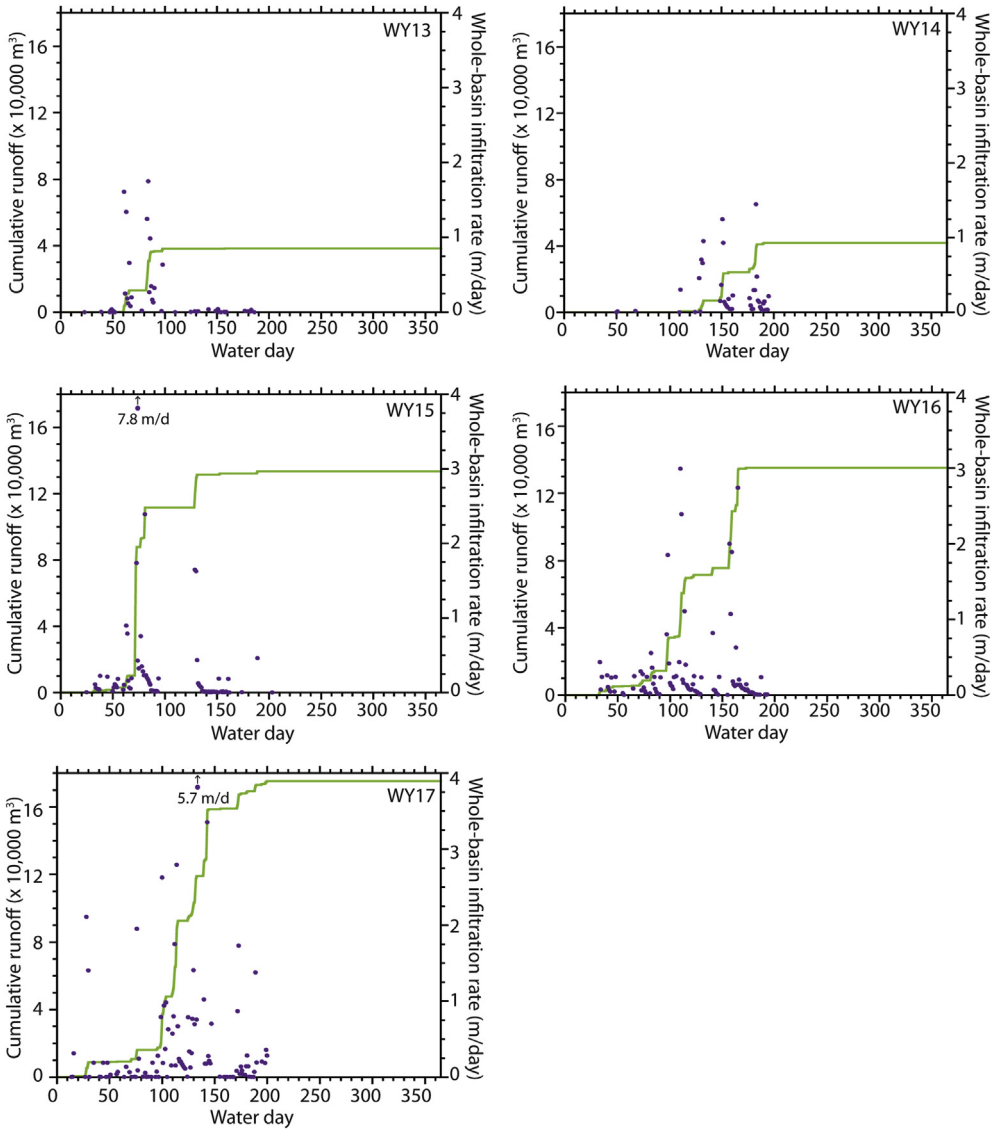

Fig. 5. Basin-average, daily infiltration rates (*right axes, dots*) were highest during periods of rapid runoff accumulation (cumulative daily runoff shown on *left axes,lines*), illustrating that system performance was runoff-limited rather than infiltration capacity–limited.

conductivity (K) of accumulating sediment was two orders of magnitude lower than the median K of surface soil. Shallow-soil effective hydraulic conductivity (K_{eff}) decreased during WY13–15 by more than two orders of magnitude (Fig. 8A–C). There was a consistent gradient in K_{eff} during WY13–15, from higher values in the north to lower values in the south, corresponding to the soil-type transition (Fig. 1B), but spatial variability in K_{eff} also decreased over time (Fig. 8).

We calculated the influence of surface sediment accumulation on K_{eff} using values from WY13 as an initial condition (Fig. 8D). Observed sediment accumulation was $\leq$8 cm/yr (Table 2) and calculated K_{eff} values decreased by up to an order of magnitude (Fig. 8D). However, observed K_{eff} during WY13–15 decreased by more than the surface-accumulation model indicated (Fig. 8A–C). This is consistent with the penetration of fine grains into shallow soils (Fig. 7C), perhaps facilitated by tilling without removing newly deposited material.

4. Discussion

In six years of operation, including a severe, multi-year drought, the DSC–MAR project infiltrated 5.3×10^5 m^3 (426 ac-ft) of water. Most of this benefit was achieved during the last three years of the study, during and soon after intense storms. This study did not quantify the fraction of infiltrated water that reached underlying aquifers, which is a challenging technical problem (Izbicki et al., 2000, 2008; Scanlon et al., 2002; Schmidt et al., 2011b). Some infiltrated water may become ET or fill unsaturated pores, never reaching the water table. However, ET losses appear to be small in this study, as was found at the Harkins Slough MAR site (Racz et al., 2011). DSC–MAR projects are intended to operate during rainy periods, when the air is humid and shallow soils contain significant moisture from earlier precipitation, so ET losses are likely modest. The fraction of infiltration that eventually becomes recharge will likely increase over each operating season, with the most recent infiltration helping drive water infiltrated during previous storms

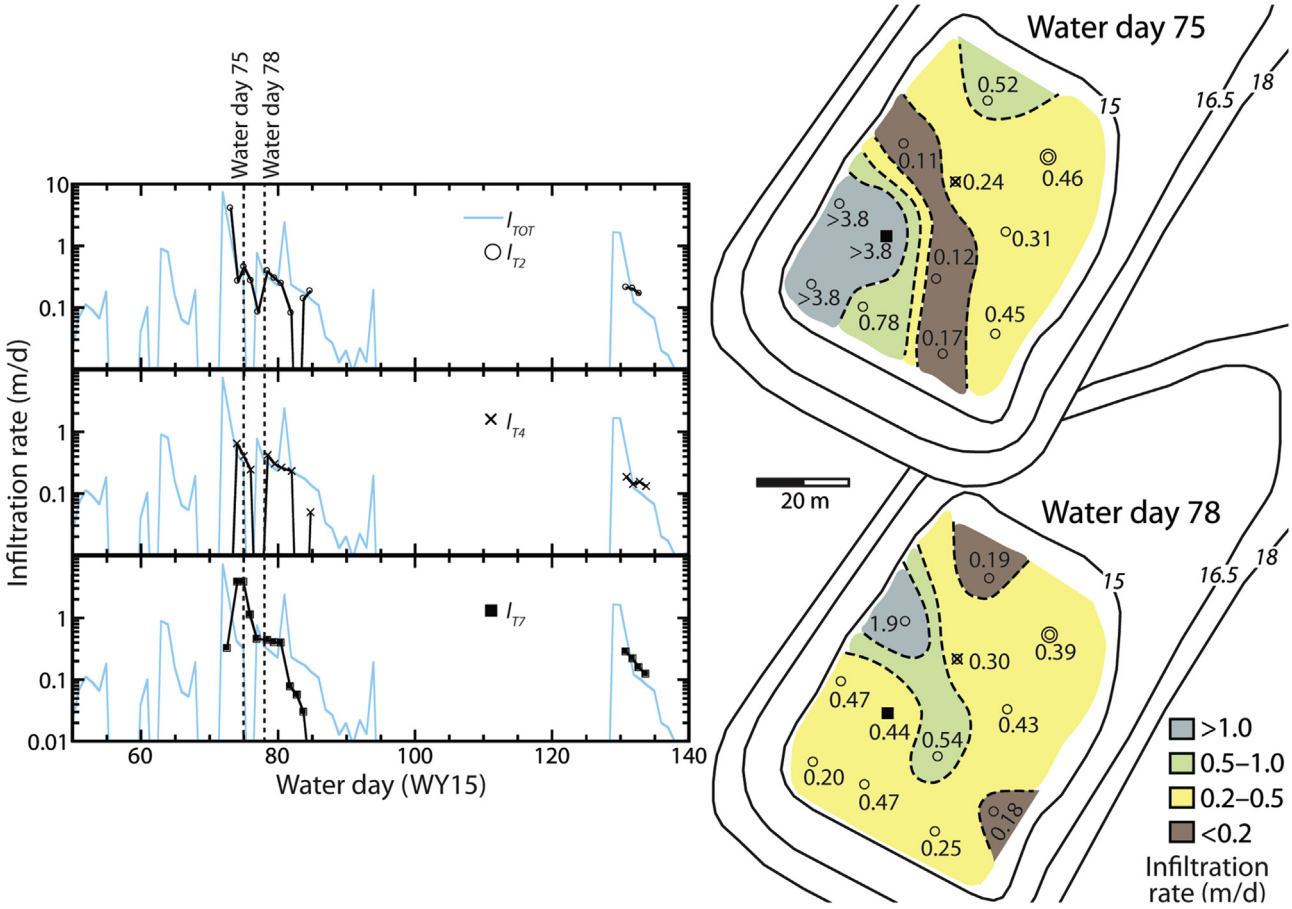

Fig. 6. Point-specific infiltration rates at three basin locations (*left*) were often lower than basin-average rates (*blue*). Contour plots of infiltration rates at twelve locations (*right*) show that the spatial distribution of infiltration rates shifted over several days. The symbols in the left panels correspond to locations on the contour maps. Elevation contours are in m-msl; infiltration rate contours are in m/d. (For interpretation of the references to colour in this figure legend, the reader is referred to the web version of this article.)

into underlying aquifers.

Runoff can transport and deposit fine-grained sediment into infiltration structures, which could limit the long-term effectiveness of DSC–MAR projects. In the present study, 8.2×10^5 kg (900 tons) of fine-grained sediment accumulated in the infiltration basin over WY13–15. K_{eff} in the infiltration basin decreased by more than two orders of magnitude (Fig. 8) due to both surface and subsurface fine-grain accumulation. Similarly, at the Harkins Slough MAR site, soil conductivity decreased by two orders of magnitude over 80 days due to sediment accumulation (Racz et al., 2011). Basin-average infiltration rates did not show a consistent long-term trend during this study, perhaps because system performance was runoff-limited rather than infiltration capacity–limited (Fig. 5). It may also be that fast infiltration pathways were maintained despite significant sediment accumulation. Plants cover much of the basin during the wet season, helping sustain an open soil structure that could allow infiltrating water to bypass a surface clogging layer.

Rainfall timing and intensity help explain annual variations in runoff sediment load (Table 2). For example, runoff sediment load was more than five times greater in WY13 than WY14. Most precipitation (and all runoff) in WY13 came early in the wet season, whereas most precipitation (and all runoff) in WY14 came late in the wet season (Fig. 2), when well-developed crops and other vegetation may have stabilized soil and reduced the amount of sediment available for transport. Carefully managing sediment as part of MAR operations is critical to maintain long-term effectiveness (Behnke, 1969; Okubo and Matsumoto, 1983; Schuh, 1990; Vandevivere et al., 1995; Bekele et al., 2013; Barraud et al., 2014). Beneficial practices include applying source control measures to reduce erosion in the drainage area, retaining sediment in a detention basin with adequate size and residence time, and/or removing accumulated fine sediment annually (prior to tilling).

Site selection is also crucial for DSC–MAR project success. Infiltration basins are strongly influenced by subtle differences in shallow soils (Fig. 1B). A recent GIS analysis of soil and aquifer conditions in the PVGB found that 7% of the region (15 km^2; 3800 ac) has surface and subsurface conditions highly suitable for MAR (Russo et al., 2014). The DSC–MAR project in the present study is in a small area classified as moderately suitable, and is surrounded by a larger, much less suitable region. Land that is less suitable for MAR due to low infiltration capacity can be part of a successful DSC–MAR project by generating runoff. In this regard, a heterogeneous region may be ideal for generating and infiltrating runoff through DSC–MAR.

There are concerns that MAR could adversely impact groundwater quality in some settings (Barraud et al., 1999; Page et al., 2010; Nandha et al., 2015; Newland, 2015). However, in extensively irrigated agricultural regions that suffer from persistent overdraft, there is inherent risk (and arguably guaranteed harm) in not actively recharging surface water. Overdraft can lower

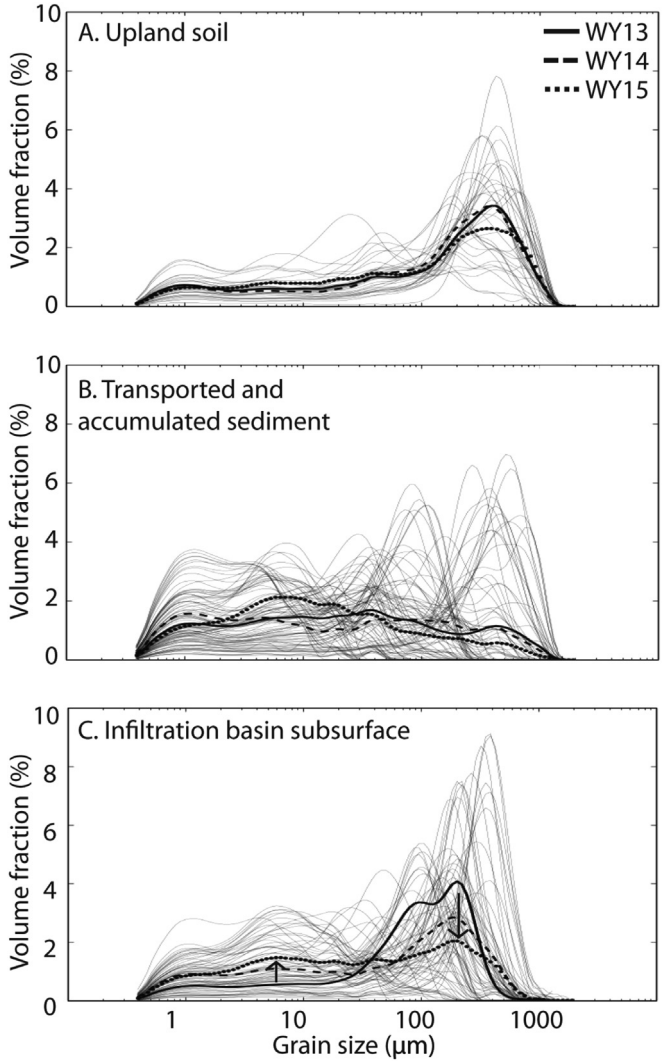

Fig. 7. Grain size distributions of upland soil (**A**), transported and accumulated sediment (**B**), and infiltration basin subsurface (**C**). *Arrows* in **C** indicate a relative increase in the proportion of fine grains, and decrease in the proportion of coarse grains, in the infiltration basin subsurface over time. *Thick lines* represent mean distributions for WY13–15.

groundwater levels and disconnect pathways by which salts and nutrients are flushed from aquifers, making them a terminal sink for contaminants. By increasing recharge, DSC–MAR projects can dilute contaminants in aquifers and reconnect groundwater and surface water, restoring flows that remove dissolved solutes.

Groundwater quality can also be improved when contaminants, such as nitrate, are removed from infiltrating water during MAR (Greskowiak et al., 2005; Schmidt et al., 2011b). Nitrate is a pervasive contaminant in many agricultural basins, yet it is challenging to remove from shallow groundwater (Böhlke and Denver, 1995; Fryar et al., 2000; Böhlke et al., 2002; Burow et al., 2008). At the Harkins Slough MAR site, rapid denitrification was observed in shallow soils when the infiltration rate was $\leq$0.7 m/d (Schmidt et al., 2011a). In the present study, full-basin and point-specific infiltration rates crossed back and forth across this threshold (Fig. 6). We did not analyze water quality in this study, but laboratory and field studies of interconnected hydrological, geochemical, and microbial processes are underway and will inform DSC–MAR design and operation for simultaneous benefit to water supply and quality.

5. Implications and conclusions

DSC–MAR can be an effective and low-cost strategy for improving groundwater resources in the PVGB, even during a severe drought. This approach is likely applicable in other regions, with modifications based on local soil and aquifer conditions, hydrology, and social constraints (e.g., permitting, water rights, economic considerations). While regional mapping and modeling can help identify the best locations for DSC–MAR, there is no substitute for direct field observations to verify model predictions and validate performance. An instrumentation network including real-time data telemetry provides a useful way to monitor DSC–MAR operations, assess benefits, evaluate potential risks (e.g., flooding), and communicate with project partners and regional stakeholders.

It can be challenging to predict runoff generation and DSC–MAR performance using conventional metrics for annual, monthly, or even daily precipitation. High-resolution precipitation data show that individual storms in the PVGB are highly variable in depth, duration, and intensity, leading to significant variation in how water is routed once it meets the landscape. A nuanced understanding of sub-daily precipitation is required to predict how much runoff will be generated during each storm and how a DSC–MAR project will respond to rapid inflow. Careful sizing of DSC–MAR project components is critical to avoid routing bottlenecks, maximizing benefits and minimizing risks.

Agricultural drainage areas may generate runoff with especially high sediment loads. In this study, the finer fraction of mobilized upland sediments accumulated in the infiltration basin, with disproportionate loss of coarser material during transport. The increasing fraction of fine-grained sediment observed in shallow soils likely reduced soil hydraulic conductivity over time. This process could be mitigated with better source control, a larger sediment detention basin, and/or regular removal of accumulated sediment. Regional soil analyses can maximize DSC–MAR benefits by identifying high–infiltration capacity features and providing information about upland sediment sources. At a small scale, vegetation in an infiltration basin may contribute fast pathways, helping reduce the impact of sediment accumulation.

Progressive sediment accumulation and soil heterogeneity at the field site contributed to widely variable infiltration rates in space and time. Understanding site-specific infiltration dynamics is critical for maximizing benefits to water supply and quality. Further exploration and quantification of relationships between hydrologic, geochemical, and microbial processes could facilitate water quality improvement during DSC–MAR.

A network of DSC–MAR projects around the PVGB, routing and infiltrating runoff during intense precipitation, would provide numerous benefits. Ten projects, each providing $\geq 1.2 \times 10^5$ m^3/yr ($\geq$100 ac-ft/yr) of infiltration, would reduce the regional water supply deficit by ~10% and could improve water quality, engage regional stakeholders, enhance aquatic habitat, and mitigate flood flows on properties and in adjacent channels. A DSC–MAR network offers several benefits relative to a centralized MAR system: DSC–MAR spreads infiltration and recharge across a broad region, focuses on sites where conditions are most favorable, takes advantage of natural precipitation and flow pathways, and can be developed and operated at relatively low cost. DSC–MAR shares advantages with similar practices, including farm field flooding and flood plain reoccupation, but could also be applied in urban and public spaces. Additional DSC–MAR field studies, including various sizes, settings, and design/operational plans, will further our understanding of the most effective, long-term ways to secure reliable groundwater supplies.

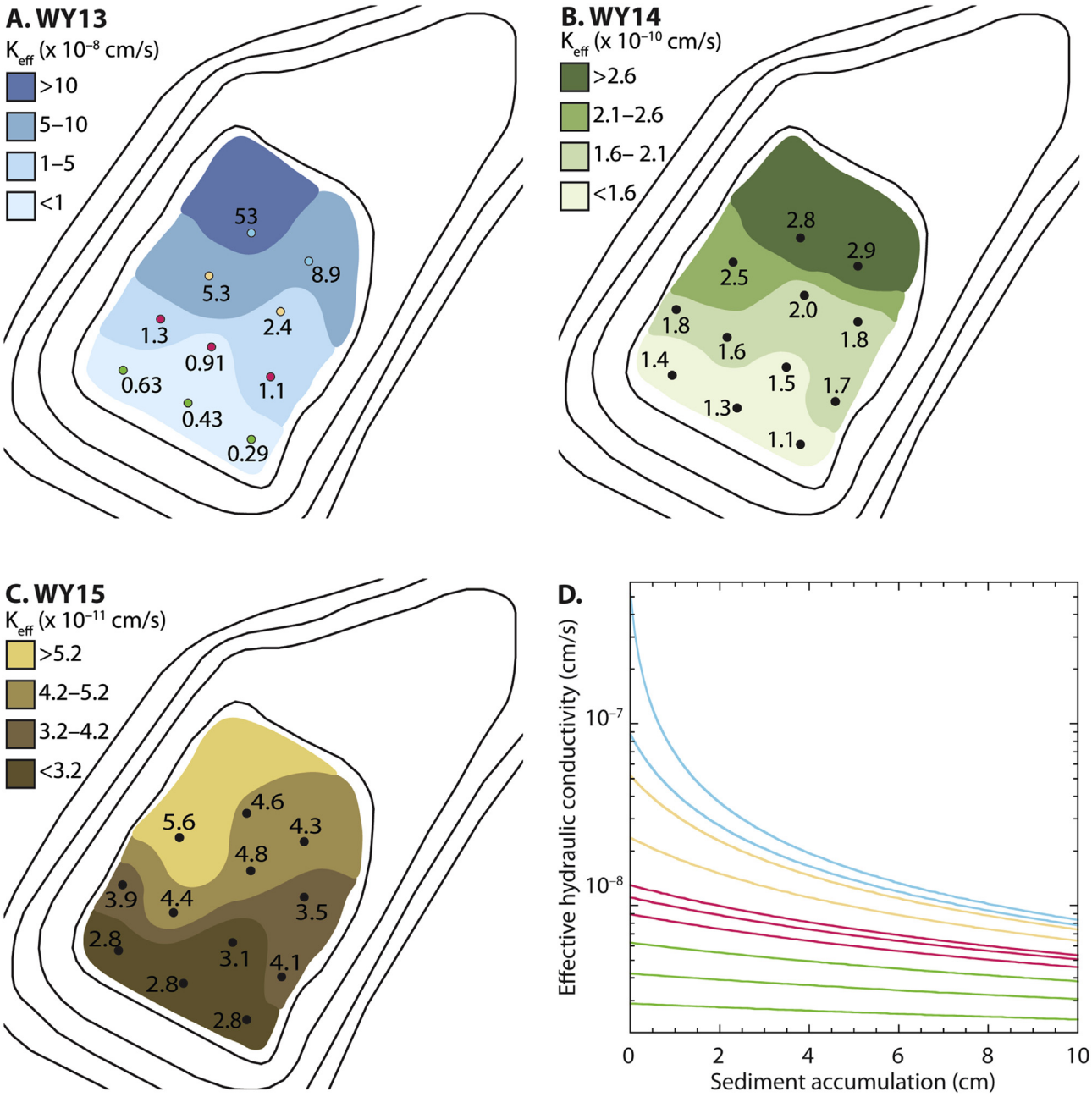

Fig. 8. Effective hydraulic conductivity of shallow soils in the infiltration basin (K_{eff}) decreased by more than two orders of magnitude over WY13–15 (**A**–**C**). Calculated K_{eff} values due to fine-grained sediment accumulation on the ground surface (**D**) varied depending on initial conditions (assigned from the start of WY13) and decreased by up to an order of magnitude with 10 cm accumulation. Colors in **D** correspond to locations in **A**.

Acknowledgments and data

We thank project landowners and tenants, staff of the Resource Conservation District of Santa Cruz County, and Driscoll's personnel for their cooperation and collaboration in operating and providing access to the DSC–MAR project. M. Los Huertos was a co-leader in launching this project and establishing and operating the measurement and sampling network during the first two project years. We are grateful for technical, field, and lab support provided by B. Cheney, B. Groza, D. Hamblin, R. Harmon, C. Hill, C. Hirota, N. Jacuzzi, K. Camara, R. Lauer, E. Lujan, B. Montgomery, E. Oleynic, E. Paddock, S. Perez, A. Racz, T. Russo, N. Strong-Cvetich, S. Sadeghi, D. Sampson, T. Sproule, C. Steinmetz, T. Stewart, C. Torres, D. Van den Dries, A. Vanden Hout, T. Weathers, W. Weir, A. Weisenberger, and D. Winslow.

All data recorded/generated by the authors (including precipitation, runoff, mass balance, sediment accumulation, site survey, grain size, and point-specific infiltration rates) are available at https://dash.library.ucsc.edu/stash/dataset/doi:10.7291/D13W28. Additional precipitation and PET data were downloaded from the California Irrigation Management Information System (http://www.cimis.water.ca.gov/); soils data from Natural Resources Conservation Service Soils Database (https://gdg.sc.egov.usda.gov/GDGOrder.aspx); and digital elevation models (DEMs) from the U.S. Geological Survey (https://viewer.nationalmap.gov/viewer/).

This research was funded by the University of California Water

Security and Sustainability Research Initiative (#449214-RB-69085), supported by the UC Office of the President's Multi-Campus Research Programs and Initiatives (MR-15-328473); the Gordon and Betty Moore Foundation (Grant GBMF5595 to A. Fisher and C. Saltikov); the California Institute for Water Resources (#SA7750); a Graduate Research Fellowship from the US National Science Foundation; a Charles and Jennifer Lawson Hydrology Award (UC Santa Cruz); and a John Mason Clarke 1877 Fellowship (Amherst College).

Appendix A. Supplementary data

Supplementary data related to this article can be found at http://dx.doi.org/10.1016/j.jenvman.2017.05.058.

References

Akgiray, Ö., 2005. Explicit solutions of the Manning equation for partially filled circular pipes. Can. J. Civ. Eng. 32 (3), 490–499. http://dx.doi.org/10.1139/l05-001.

Anderson, M.P., 2005. Heat as a groundwater tracer. Ground Water 43 (6), 951–968. http://dx.doi.org/10.1111/j.1745-6584.2005.00052.x.

Asner, G.P., Brodrick, P.G., Anderson, C.B., Vaughn, N., Knapp, D.E., Martin, R.E., 2016. Progressive forest canopy water loss during the 2012–2015 California drought. Proc. Natl. Acad. Sci. 113 (2), E249–E255. http://dx.doi.org/10.1073/pnas.1523397113.

Barraud, S., Gautier, A., Bardin, J.P., Riou, V., 1999. The impact of intentional stormwater infiltration on soil and groundwater. Water Sci. Technol. 39 (2), 185–192.

Barraud, S., Gonzalez-Merchan, C., Nascimento, N., Moura, P., Silva, A., 2014. A method for evaluating the evolution of clogging: application to the Pampulha Campus infiltration system (Brazil). Water Sci. Technol. 69 (6), 1241,. http://dx.doi.org/10.2166/wst.2013.819.

Behnke, J., 1969. Clogging in surface spreading operations for artifical ground-water recharge. Water Resour. Res. 5 (4), 870–876.

Bekele, E., Toze, S., Patterson, B., Fegg, W., Shackleton, M., Higginson, S., 2013. Evaluating two infiltration gallery designs for managed aquifer recharge using secondary treated wastewater. J. Environ. Manag. 117, 115–120. http://dx.doi.org/10.1016/j.jenvman.2012.12.018.

Bhaskar, A.S., Hogan, D.M., Archfield, S.A., 2016. Urban base flow with low impact development: urban base flow with low impact development. Hydrol. Process. 30 (18), 3156–3171. http://dx.doi.org/10.1002/hyp.10808.

Böhlke, J.K., Denver, J.M., 1995. Combined use of groundwater dating, chemical, and isotopic analyses to resolve the history and fate of nitrate contamination in two agricultural watersheds, Atlantic Coastal Plain, Maryland. Water Resour. Res. 31 (9), 2319–2339. http://dx.doi.org/10.1029/95WR01584.

Böhlke, J.K., Wanty, R., Tuttle, M., Delin, G., Landon, M., 2002. Denitrification in the recharge area and discharge area of a transient agricultural nitrate plume in a glacial outwash sand aquifer, Minnesota. Water Resour. Res. 38 (7) http://dx.doi.org/10.1029/2001WR000663, 10–1-10–26.

Bouwer, H., 1999. Artificial Recharge of Groundwater: Systems, Design, and Management, Hydraulic Design Handbook. McGraw-Hill, New York, pp. 24–31.

Bouwer, H., 2002. Artificial recharge of groundwater: hydrogeology and engineering. Hydrogeol. J. 10 (1), 121–142. http://dx.doi.org/10.1007/s10040-001-0182-4.

Burow, K.R., Shelton, J.L., Dubrovsky, N.M., 2008. Regional nitrate and pesticide trends in ground water in the Eastern San Joaquin Valley, California. J. Environ. Qual. 37, 249–263. http://dx.doi.org/10.2134/jeq2007.0061.

California Department of Water Resources, 1998a. California Water Plan Update. California Department of Water Resources, Sacramento, CA.

California Department of Water Resources, 1998b. Technical Elements of CIMIS. The California Irrigation Management Information SystemRep.

California Department of Water Resources, 2013. California Water Plan, Update 2013. California Department of Water Resources, Sacramento, CA.

Cantone, J., Schmidt, A., 2011. Improved understanding and prediction of the hydrologic response of highly urbanized catchments through development of the Illinois Urban Hydrologic Model. Water Resour. Res. 47 (8) http://dx.doi.org/10.1029/2010WR009330 n/a-n/a.

Chaffin, B.C., Shuster, W.D., Garmestani, A.S., Furio, B., Albro, S.L., Gardiner, M., Spring, M., Green, O.O., 2016. A tale of two rain gardens: barriers and bridges to adaptive management of urban stormwater in Cleveland, Ohio. J. Environ. Manag. 183, 431–441. http://dx.doi.org/10.1016/j.jenvman.2016.06.025.

Chapuis, R.P., 2012. Predicting the saturated hydraulic conductivity of soils: a review. Bull. Eng. Geol. Environ. 71 (3), 401–434. http://dx.doi.org/10.1007/s10064-012-0418-7.

Chapuis, R.P., Aubertin, M., 2003. On the use of the Kozeny Carman equation to predict the hydraulic conductivity of soils. Can. Geotech. J. 40 (3), 616–628.

Chen, Y., Samuelson, H.W., Tong, Z., 2016. Integrated design workflow and a new tool for urban rainwater management. J. Environ. Manag. 180, 45–51. http://dx.doi.org/10.1016/j.jenvman.2016.04.059.

Chenini, I., Mammou, A.B., El May, M., 2010. Groundwater recharge zone mapping using GIS-based multi-criteria analysis: a case study in central Tunisia (Maknassy Basin). Water Resour. Manag. 24 (5), 921–939. http://dx.doi.org/10.1007/s11269-009-9479-1.

Clark, J.F., Hudson, G.B., Davisson, M.L., Woodside, G., Herndon, R., 2004. Geochemical imaging of flow near an artificial recharge facility, Orange County, California. Ground Water 42 (2), 167–174.

Constantz, J., 2008. Heat as a tracer to determine streambed water exchanges. Water Resour. Res. 44 (4) http://dx.doi.org/10.1029/2008WR006996.

Constantz, J., Thomas, C.L., 1996. The use of streambed temperature profiles to estimate the depth, duration, and rate of percolation beneath arroyos. Water Resour. Res. 32 (12), 3597–3602. http://dx.doi.org/10.1029/96WR03014.

Dillon, P., 2005. Future management of aquifer recharge. Hydrogeol. J. 13 (1), 313–316. http://dx.doi.org/10.1007/s10040-004-0413-6.

Dillon, P., Toze, S., Page, D., Vanderzalm, J., Bekele, E., Sidhu, J., Rinck-Pfeiffer, S., 2010. Managed aquifer recharge: rediscovering nature as a leading edge technology. Water Sci. Technol. 62 (10), 2338,. http://dx.doi.org/10.2166/wst.2010.444.

Döll, P., Müller Schmied, H., Schuh, C., Portmann, F.T., Eicker, A., 2014. Global-scale assessment of groundwater depletion and related groundwater abstractions: combining hydrological modeling with information from well observations and GRACE satellites. Water Resour. Res. 50 (7), 5698–5720. http://dx.doi.org/10.1002/2014WR015595.

Doussan, C., Ledoux, E., Detay, M., 1998. River-groundwater exchanges, bank filtration, and groundwater quality: ammonium behavior. J. Environ. Qual. 27, 1418–1427.

Dunkerley, D., 2008. Identifying individual rain events from pluviograph records: a review with analysis of data from an Australian dryland site. Hydrol. Process. 22 (26), 5024–5036. http://dx.doi.org/10.1002/hyp.7122.

Dunne, T., Black, R.D., 1970. Partial area contributions to storm runoff in a small New England watershed. Water Resour. Res. 6 (5), 1296–1311.

Faunt, C.C., Sneed, M., Traum, J., Brandt, J.T., 2016. Water availability and land subsidence in the Central Valley, California, USA. Hydrogeol. J. 24 (3), 675–684. http://dx.doi.org/10.1007/s10040-015-1339-x.

Ficklin, D.L., Luo, Y., Luedeling, E., Gatzke, S.E., Zhang, M., 2010. Sensitivity of agricultural runoff loads to rising levels of CO2 and climate change in the San Joaquin Valley watershed of California. Environ. Pollut. 158 (1), 223–234. http://dx.doi.org/10.1016/j.envpol.2009.07.016.

Fryar, A.E., Macko, S.A., Mullican, W.F.I., Romanak, K.D., Bennett, P.C., 2000. Nitrate reduction during ground-water recharge, southern high plains, Texas. J. Contam. Hydrol. 40, 335–363.

Furl, C., Sharif, H.O., Alzahrani, M., El Hassan, A., Mazari, N., 2014. Precipitation amount and intensity trends across southwest Saudi Arabia. JAWRA J. Am. Water Resour. Assoc. 50 (1), 74–82. http://dx.doi.org/10.1111/jawr.12118.

Galloway, D.L., Hudnut, K.W., Ingebritsen, S.E., Phillips, S.P., Peltzer, G., Rogez, F., Rosen, P.A., 1998. Detection of aquifer system compaction and land subsidence using interferometric synthetic aperture radar, Antelope Valley, Mojave Desert, California. Water Resour. Res. 34 (10), 2573–2585.

García-Ruiz, J.M., Nadal-Romero, E., Lana-Renault, N., Beguería, S., 2013. Erosion in Mediterranean landscapes: changes and future challenges. Geomorphology 198, 20–36. http://dx.doi.org/10.1016/j.geomorph.2013.05.023.

Gleeson, T., VanderSteen, J., Sophocleous, M.A., Taniguchi, M., Alley, W.M., Allen, D.M., Zhou, Y., 2010. Groundwater sustainability strategies. Nat. Geosci. 3 (6), 378–379.

Grebel, J.E., Mohanty, S.K., Torkelson, A.A., Boehm, A.B., Higgins, C.P., Maxwell, R.M., Nelson, K.L., Sedlak, D.L., 2013. Engineered infiltration systems for urban stormwater reclamation. Environ. Eng. Sci. 30 (8), 437–454. http://dx.doi.org/10.1089/ees.2012.0312.

Greskowiak, J., Prommer, H., Massmann, G., Johnston, C.D., Nützmann, G., Pekdeger, A., 2005. The impact of variably saturated conditions on hydrogeochemical changes during artificial recharge of groundwater. Appl. Geochem. 20 (7), 1409–1426. http://dx.doi.org/10.1016/j.apgeochem.2005.03.002.

Griffin, D., Anchukaitis, K.J., 2014. How unusual is the 2012-2014 California drought? Geophys. Res. Lett. 41 (24), 9017–9023. http://dx.doi.org/10.1002/2014GL062433.

Hanson, R.T., Lockwood, B., Schmid, W., 2014a. Analysis of projected water availability with current basin management plan, Pajaro Valley, California. J. Hydrol. 519, 131–147. http://dx.doi.org/10.1016/j.jhydrol.2014.07.005.

Hanson, R.T., Schmid, W., Faunt, C.C., Lear, J., Lockwood, B., 2014b. Integrated Hydrologic Model of Pajaro Valley, Santa Cruz and Monterey Counties, California, Scientific Investigations Report. U.S. Geological Survey.

Harding ESE, 2001. Biological Assessment, Pajaro River and Salsipuedes and Corralitos Creeks, Management and Restoration Plan, Santa Cruz County, California, County of Santa Cruz, Santa Cruz, CA.

Hatch, C.E., Fisher, A.T., Revenaugh, J.S., Constantz, J., Ruehl, C., 2006. Quantifying surface water-groundwater interactions using time series analysis of streambed thermal records: method development. Water Resour. Res. 42 (10) http://dx.doi.org/10.1029/2005WR004787.

Hatch, C.E., Fisher, A.T., Ruehl, C.R., Stemler, G., 2010. Spatial and temporal variations in streambed hydraulic conductivity quantified with time-series thermal methods. J. Hydrol. 389 (3–4), 276–288. http://dx.doi.org/10.1016/j.jhydrol.2010.05.046.

Horton, R.E., 1933. The role of infiltration in the hydrologic cycle. Eos, Trans. Am. Geophys. Union 14 (1), 446–460.

Izbicki, J.A., Radyk, J., Michel, R.L., 2000. Water movement through a thick

unsaturated zone underlying an intermittent stream in the western Mojave Desert, southern California, USA. J. Hydrol. 238, 194–217.
Izbicki, J.A., Flint, A.L., Stamos, C.L., 2008. Artificial recharge through a thick, heterogeneous unsaturated zone. Ground Water 46 (3), 475–488. http://dx.doi.org/10.1111/j.1745-6584.2007.00406.x.
Jha, M.K., Chowdhury, A., Chowdary, V.M., Peiffer, S., 2007. Groundwater management and development by integrated remote sensing and geographic information systems: prospects and constraints. Water Resour. Manag. 21 (2), 427–467. http://dx.doi.org/10.1007/s11269-006-9024-4.
Jia, Z., Tang, S., Luo, W., Li, S., Zhou, M., 2016. Small scale green infrastructure design to meet different urban hydrological criteria. J. Environ. Manag. 171, 92–100. http://dx.doi.org/10.1016/j.jenvman.2016.01.016.
Jong, B.-T., Ting, M., Seager, R., 2016. El Niño's impact on California precipitation: seasonality, regionality, and El Niño intensity. Environ. Res. Lett. 11 (5), 54021,. http://dx.doi.org/10.1088/1748-9326/11/5/054021.
Kaźmierczak, B., Kotowski, A., 2014. The influence of precipitation intensity growth on the urban drainage systems designing. Theor. Appl. Climatol. 118 (1–2), 285–296. http://dx.doi.org/10.1007/s00704-013-1067-x.
Koluvek, P.K., Tanji, K.K., Trout, T.J., 1993. Overview of soil erosion from irrigation. J. Irrig. Drain. Eng. 119 (6), 929–946.
Konikow, L.F., Kendy, E., 2005. Groundwater depletion: a global problem. Hydrogeol. J. 13 (1), 317–320. http://dx.doi.org/10.1007/s10040-004-0411-8.
Leahy, P.G., Kiely, G., 2011. Short duration rainfall extremes in Ireland: influence of climatic variability. Water Resour. Manag. 25 (3), 987–1003. http://dx.doi.org/10.1007/s11269-010-9737-2.
Lee, T.-C., Williams, A.E., Wang, C., 1992. An artificial recharge experiment in the San Jacinto basin, Riverside, southern California. J. Hydrol. 140 (1–4), 235–259.
Lenderink, G., van Meijgaard, E., 2008. Increase in hourly precipitation extremes beyond expectations from temperature changes. Nat. Geosci. 1 (8), 511–514. http://dx.doi.org/10.1038/ngeo262.
Li, H.-Y., Sivapalan, M., Tian, F., Harman, C., 2014. Functional approach to exploring climatic and landscape controls of runoff generation: 1. Behavioral constraints on runoff volume. Water Resour. Res. 50 (12), 9300–9322. http://dx.doi.org/10.1002/2014WR016307.
Liu, S.C., Fu, C., Shiu, C.-J., Chen, J.-P., Wu, F., 2009. Temperature dependence of global precipitation extremes. Geophys. Res. Lett. 36 (17) http://dx.doi.org/10.1029/2009GL040218.
Ma, L., Spalding, R.F., 1997. Effects of artifical recharge on ground water quality and aquifer storange recovery. J. Am. Water Resour. Assoc. 33 (3).
Mahlstein, I., Portmann, R.W., Daniel, J.S., Solomon, S., Knutti, R., 2012. Perceptible changes in regional precipitation in a future climate. Geophys. Res. Lett. 39, L05701. http://dx.doi.org/10.1029/2011GL050738.
Mann, M.E., Gleick, P.H., 2015. Climate change and California drought in the 21st century. Proc. Natl. Acad. Sci. 112 (13), 3858–3859. http://dx.doi.org/10.1073/pnas.1503667112.
Massey, F.J., 1951. The Kolmogorov-Smirnov test for goodness of fit. J. Am. Stat. Assoc. 46 (253), 68,. http://dx.doi.org/10.2307/2280095.
Min, S.-K., Zhang, X., Zwiers, F.W., Hegerl, G.C., 2011. Human contribution to more-intense precipitation extremes. Nature 470 (7334), 378–381. http://dx.doi.org/10.1038/nature09763.
Nandha, M., Berry, M., Jefferson, B., Jeffrey, P., 2015. Risk assessment frameworks for MAR schemes in the UK. Environ. Earth Sci. 73 (12), 7747–7757. http://dx.doi.org/10.1007/s12665-014-3399-y.
National Research Council, 2008. Urban Stormwater Management in the United States. National Academies Press, Washington, DC.
Nelson, R.L., 2012. Assessing local planning to control groundwater depletion: California as a microcosm of global issues. Water Resour. Res. 48 (1) http://dx.doi.org/10.1029/2011WR010927.
Nenna, V., Herckenrath, D., Knight, R., Odlum, N., McPhee, D., 2013. Application and evaluation of electromagnetic methods for imaging saltwater intrusion in coastal aquifers: Seaside Groundwater Basin, California. Geophysics 78 (2), B77–B88. http://dx.doi.org/10.1190/geo2012-0004.1.
Newcomer, M.E., Gurdak, J.J., Sklar, L.S., Nanus, L., 2014. Urban recharge beneath low impact development and effects of climate variability and change. Water Resour. Res. 50 (2), 1716–1734. http://dx.doi.org/10.1002/2013WR014282.
Newland, P.Q., 2015. The development, application and acceptance of environmental and health risk assessment methodology for MAR schemes in South Australia. Environ. Earth Sci. 73 (12), 7739–7745. http://dx.doi.org/10.1007/s12665-014-3406-3.
NOAA Fisheries, 2016. Steelhead Trout (Oncorhynchus mykiss). Available from: http://www.fisheries.noaa.gov/pr/species/fish/steelhead-trout.html (Accessed 26 September 2016).
O'Geen, A.T., et al., 2015. Soil suitability index identifies potential areas for groundwater banking on agricultural lands. Calif. Agric. 69 (2), 75–84. http://dx.doi.org/10.3733/ca.v069n02p75.
Okubo, T., Matsumoto, J., 1983. Biological clogging of sand and changes of organic constituents during artificial recharge. Water Res. 17 (7), 813–821.
Page, D., Dillon, P., Vanderzalm, J., Toze, S., Sidhu, J., Barry, K., Levett, K., Kremer, S., Regel, R., 2010. Risk assessment of aquifer storage transfer and recovery with urban stormwater for producing water of a potable quality. J. Environ. Qual. 39 (6), 2029,. http://dx.doi.org/10.2134/jeq2010.0078.
Pajaro Valley Water Management Agency, 2014. Basin Management Plan Update, Final: February 2014. Pajaro Valley Water Management Agency, Watsonville, CA.
Pavelic, P., Dillon, P.J., Barry, K.E., Gerges, N.Z., 2006. Hydraulic evaluation of aquifer storage and recovery (ASR) with urban stormwater in a brackish limestone aquifer. Hydrogeol. J. 14 (8), 1544–1555. http://dx.doi.org/10.1007/s10040-006-0078-4.
Quast, K.W., Lansey, K., Arnold, R., Bassett, R.L., Rincon, M., 2006. Boron isotopes as an artificial tracer. Ground Water 44 (3), 453–466. http://dx.doi.org/10.1111/j.1745-6584.2006.00186.x.
Racz, A.J., Fisher, A.T., Schmidt, C.M., Lockwood, B.S., Los Huertos, M., 2011. Spatial and temporal infiltration dynamics during managed aquifer recharge. Groundwater 50 (4), 562–570. http://dx.doi.org/10.1111/j.1745-6584.2011.00875.x.
Rahman, M.A., Rusteberg, B., Gogu, R.C., Lobo Ferreira, J.P., Sauter, M., 2012. A new spatial multi-criteria decision support tool for site selection for implementation of managed aquifer recharge. J. Environ. Manag. 99, 61–75. http://dx.doi.org/10.1016/j.jenvman.2012.01.003.
Rahman, M.A., Rusteberg, B., Uddin, M.S., Lutz, A., Saada, M.A., Sauter, M., 2013. An integrated study of spatial multicriteria analysis and mathematical modelling for managed aquifer recharge site suitability mapping and site ranking at Northern Gaza coastal aquifer. J. Environ. Manag. 124, 25–39. http://dx.doi.org/10.1016/j.jenvman.2013.03.023.
Richey, A.S., Thomas, B.F., Lo, M.-H., Reager, J.T., Famiglietti, J.S., Voss, K., Swenson, S., Rodell, M., 2015. Quantifying renewable groundwater stress with GRACE. Water Resour. Res. 51 (7), 5217–5238. http://dx.doi.org/10.1002/2015WR017349.
Ruehl, C., Fisher, A.T., Hatch, C., Los Huertos, M., Stemler, G., Shennan, C., 2006. Differential gauging and tracer tests resolve seepage fluxes in a strongly-losing stream. J. Hydrol. 330 (1–2), 235–248. http://dx.doi.org/10.1016/j.jhydrol.2006.03.025.
Russo, T.A., Fisher, A.T., Winslow, D.M., 2013. Regional and local increases in storm intensity in the san Francisco Bay area, USA, between 1890 and 2010. J. Geophys. Res. Atmos. 118 (8), 3392–3401. http://dx.doi.org/10.1002/jgrd.50225.
Russo, T.A., Fisher, A.T., Lockwood, B.S., 2014. Assessment of managed aquifer recharge site suitability using a GIS and modeling. Groundwater 53 (3), 389–400. http://dx.doi.org/10.1111/gwat.12213.
Saraf, A.K., Choudhury, P.R., 1998. Integrated remote sensing and GIS for groundwater exploration and identification of artificial recharge sites. Int. J. Remote Sens. 19 (10), 1825–1841. http://dx.doi.org/10.1080/014311698215018.
Scanlon, B.R., Healy, R.W., Cook, P.G., 2002. Choosing appropriate techniques for quantifying groundwater recharge. Hydrogeol. J. 10 (1), 18–39.
Scanlon, B.R., Reedy, R.C., Faunt, C.C., Pool, D., Uhlman, K., 2016. Enhancing drought resilience with conjunctive use and managed aquifer recharge in California and Arizona. Environ. Res. Lett. 11 (4), 49501,. http://dx.doi.org/10.1088/1748-9326/11/4/049501.
Schmidt, C.M., Fisher, A.T., Racz, A.J., Lockwood, B.S., Huertos, M.L., 2011a. Linking denitrification and infiltration rates during managed groundwater recharge. Environ. Sci. Technol. 45 (22), 9634–9640. http://dx.doi.org/10.1021/es2023626.
Schmidt, C.M., Fisher, A.T., Racz, A., Wheat, C.G., Los Huertos, M., Lockwood, B., 2011b. Rapid nutrient load reduction during infiltration of managed aquifer recharge in an agricultural groundwater basin: Pajaro Valley, California. Hydrol. Process. 26 (15), 2235–2247.
Schuh, W.M., 1990. Seasonal variation of clogging of an artificial recharge basin in a northern climate. J. Hydrol. 121 (1), 193–215.
Shang, H., Yan, J., Zhang, X., 2011. El Niño-Southern Oscillation influence on winter maximum daily precipitation in California in a spatial model. Water Resour. Res. 47 (11) http://dx.doi.org/10.1029/2011WR010415.
Soil Survey Staff, U.S. Department of Agriculture, 2014. Soil Survey Geographic (SSURGO) Database. Available from: https://gdg.sc.egov.usda.gov/GDGOrder.aspx.
Stephens, D.B., Miller, M., Moore, S.J., Umstot, T., Salvato, D.J., 2012. Decentralized groundwater recharge systems using roofwater and stormwater runoff. J. Am. Water Resour. Assoc. 48 (1).
Tomozeiu, R., Busuioc, A., Marletto, V., Zinoni, F., Cacciamani, C., 2000. Detection of changes in the summer precipitation time series of the region Emilia-Romagna, Italy. Theor. Appl. Climatol. 67 (3–4), 193–200.
Tu, J.-Y., Chou, C., 2013. Changes in precipitation frequency and intensity in the vicinity of Taiwan: typhoon versus non-typhoon events. Environ. Res. Lett. 8 (1), 14023,. http://dx.doi.org/10.1088/1748-9326/8/1/014023.
U.S. Geological Survey, 2014. Watershed boundary dataset (WBD). Available from: http://datagateway.nrcs.usda.gov.
Vandevivere, P., Baveye, P., Sanchez de Lozada, D., DeLeo, P., 1995. Microbial clogging of saturated soils and aquifer materials: evaluation of mathematical models. Water Resour. Res. 31 (9), 2173–2180.
de Vente, J., Poesen, J., 2005. Predicting soil erosion and sediment yield at the basin scale: scale issues and semi-quantitative models. Earth Sci. Rev. 71 (1–2), 95–125. http://dx.doi.org/10.1016/j.earscirev.2005.02.002.
Wada, Y., van Beek, L.P.H., van Kempen, C.M., Reckman, J.W.T.M., Vasak, S., Bierkens, M.F.P., 2010. Global depletion of groundwater resources. Geophys. Res. Lett. 37 (20) http://dx.doi.org/10.1029/2010GL044571 n/a-n/a.
Wada, Y., van Beek, L.P.H., Bierkens, M.F.P., 2012. Nonsustainable groundwater sustaining irrigation: a global assessment. Water Resour. Res. 48 http://dx.doi.org/10.1029/2011WR010562.
Werner, A.D., Bakker, M., Post, V.E.A., Vandenbohede, A., Lu, C., Ataie-Ashtiani, B., Simmons, C.T., Barry, D.A., 2013. Seawater intrusion processes, investigation and management: recent advances and future challenges. Adv. Water Resour. 51, 3–26. http://dx.doi.org/10.1016/j.advwatres.2012.03.004.
Wierda, A., Veen, A.W.L., 1992. A rainfall simulator study of infiltration into arable

soils. Agric. Water Manag. 21 (1–2), 119–135.
Wright, D.B., Smith, J.A., Villarini, G., Baeck, M.L., 2012. Hydroclimatology of flash flooding in Atlanta. Water Resour. Res. 48 (4) http://dx.doi.org/10.1029/2011WR011371.
Yeh, H.-F., Lee, C.-H., Hsu, K.-C., Chang, P.-H., 2009. GIS for the assessment of the groundwater recharge potential zone. Environ. Geol. 58 (1), 185–195. http://dx.doi.org/10.1007/s00254-008-1504-9.
Zektser, S., Loaiciga, H.A., Wolf, J.T., 2005. Environmental impacts of groundwater overdraft: selected case studies in the southwestern United States. Environ. Geol. 47 (3), 396–404. http://dx.doi.org/10.1007/s00254-004-1164-3.
Zhang, X., Cong, Z., 2014. Trends of precipitation intensity and frequency in hydrological regions of China from 1956 to 2005. Glob. Planet. Change 117, 40–51. http://dx.doi.org/10.1016/j.gloplacha.2014.03.002.
Zhang, X., Zwiers, F.W., Hegerl, G.C., Lambert, F.H., Gillett, N.P., Solomon, S., Stott, P.A., Nozawa, T., 2007. Detection of human influence on twentieth-century precipitation trends. Nature 448 (7152), 461–465. http://dx.doi.org/10.1038/nature06025.
Zolina, O., 2014. Multidecadal trends in the duration of wet spells and associated intensity of precipitation as revealed by a very dense observational German network. Environ. Res. Lett. 9 (2), 25003,. http://dx.doi.org/10.1088/1748-9326/9/2/025003.